

Estimation of winter time NO_x emissions in Hefei, a typical inland city of China, using mobile MAX-DOAS observations

Wei Tan^a, Shaohua Zhao^f, Cheng Liu^{a,b,c,d,**}, Ka Lok Chan^{e,*}, Zhouqing Xie^{a,b,c,d}, Yu Zhu^g, Wenjing Su^b, Chengxin Zhang^b, Haoran Liu^b, Chengzhi Xing^b, Jianguo Liu^{a,c}

^a Key Lab of Environmental Optics and Technology, Anhui Institute of Optics and Fine Mechanics, Hefei Institutes of Physical Science, Chinese Academy of Sciences, Hefei, 230031, China

^b School of Earth and Space Sciences, University of Science and Technology of China, Hefei, 230026, China

^c CAS Center for Excellence in Regional Atmos. Environ., Institute of Urban Environment, Chinese Academy of Sciences, Xiamen, 361021, China

^d Anhui Province Key Laboratory of Polar Environment and Global Change, University of Science and Technology of China, Hefei, 230026, China

^e Remote Sensing Technology Institute (IMF), German Aerospace Center (DLR), Oberpfaffenhofen, Germany

^f Satellite Environment Center, State Environmental Protection Key Laboratory of Satellite Remote Sensing, Ministry of Ecology and Environment, Beijing, 100094, China

^g Anhui Environmental Monitoring Center, Hefei, 230061, China

ARTICLE INFO

Keywords:
NO_x emission
Mobile measurement
MAX-DOAS
Regional transport

ABSTRACT

In this paper, we present a quantitative determination of the NO_x emission in Hefei using mobile Multi-Axis Differential Optical Absorption Spectroscopy (MAX-DOAS) measurements. The measurements were carried out during winter time from December 2016 to February 2017. The measured NO₂ vertical column densities (VCDs) show a strong spatial gradient with higher values within the city center, indicating the majority of NO_x emission sources are located at the city center. A significant “holiday effect” was found by comparing measurements taken during weekdays and weekend. The weekend reduction is more significant in the suburban (~28%) compared to the city center (~13%). Mobile measurements of NO₂ vertical column densities (VCDs) were analyzed together with meteorological data to determine the NO_x emission by applying the loop-integral method. Detailed error analysis of the NO_x emission shows the variation of wind field and large measurement gap dominated the total error of NO_x emission calculation. The result shows the NO_x emission in Hefei during winter time varies in a wide range from 10×10^{24} to 40×10^{24} molec⁻¹ with an average of 18.44×10^{24} molec⁻¹. Our estimation is about 43% lower than the number reported in the previous emission inventory in 2012. The reduction of NO_x emission reflects the successful implementation of emission control measures in recent years. Our result also shows about 73% of the total NO_x in the city were transported from outside of the city during winter. The impacts of transported NO_x are especially large when air masses originated from heavily polluted regions, i.e. North China Plain and Yangtze River Delta. The result presented provides a better understanding of the impacts of local emissions and transportation of pollutants on the local air quality of Hefei.

1. Introduction

Nitrogen oxides (NO_x), defined as the sum of nitrogen oxide (NO) and nitrogen dioxide (NO₂), are the major pollutants in the atmosphere playing the key role in both tropospheric and stratospheric chemistry. They participate in the catalytic formation of ozone (O₃) in the troposphere, contribute to the formation of secondary aerosols (Jang and Kamens, 2001) and cause acid rain (Tzanis et al., 2009). In addition, NO₂ also contributes to radiative warming the earth's

atmosphere (Solomon et al., 1999). NO_x in high concentrations are known to be toxic to human (Seinfeld and Pandis, 2006, 2012). Compared to natural sources, anthropogenic sources (industrial emissions, power generation, and traffic emissions) contribute the large part of the total NO_x emission (Beirle et al., 2003; Lin, 2012; Lin and McElroy, 2011). The emissions of anthropogenic NO_x are mostly concentrated over densely populated areas due to intensive use of fossil fuel. Anthropogenic NO_x emission inventories are usually derived from the statistics of local information, such as road graph, industry location,

* Corresponding author. Remote Sensing Technology Institute (IMF), German Aerospace Center (DLR), Oberpfaffenhofen, Germany.

** Corresponding author. Key Lab of Environmental Optics and Technology, Anhui Institute of Optics and Fine Mechanics, Hefei Institutes of Physical Science, Chinese Academy of Sciences, Hefei, 230031, China.

E-mail addresses: chliu81@ustc.edu.cn (C. Liu), ka.chan@dlr.de (K.L. Chan).

population density, and electricity consumption, together with appropriate emission factors. Due to the rapid changes of sources, the statistic might not be up to date in rapid developing areas, like China and India. Therefore, it is important to have a precise estimation of the NO_x emissions in these areas to provide better input data for the model investigations of atmospheric chemistry.

Ground based Multi-Axis Differential Optical Absorption Spectroscopy (MAX-DOAS) is a passive remote sensing measurement technique for atmospheric aerosol and trace gas measurements. Information of trace gases can be derived from the measured scattered sun-light spectra by applying the DOAS technique (Platt and Stutz, 2008). As the experimental setup is rather simple and inexpensive, ground-based MAX-DOAS has been widely used for atmospheric aerosol and trace gas measurements (Chan et al., 2015; Clémér et al., 2010; Hendrick et al., 2014; Vlemmix et al., 2015; Xing et al., 2017). Mobile application of MAX-DOAS measurement provides indispensable spatial distribution information of atmospheric trace gases column densities. Combining with meteorological information, mobile MAX-DOAS measurement of trace gas columns can also be used for the determination of pollutants emission flux. Determination of the total emission of NO₂ (NO_x), sulfur dioxide (SO₂), formaldehyde (HCHO) and other air pollutants (Ibrahim et al., 2010; Johansson et al., 2008; Li et al., 2015; Shaiganfar et al., 2011, 2017; Wang et al., 2012; Wu et al., 2013) have been demonstrated in previous studies.

Hefei is an inland city located in the eastern part of China. It is also the provincial capital of Anhui province with the east is bounded to the Yangtze River Delta (YRD). Hefei is also a rapid developing city, with population of about 8 million. Owing to the rapid urbanization of Hefei and its surrounding cities in YRD, Hefei is facing a series of air pollution problems in recent years. As shown in Fig. 1, Hefei is surrounded by heavily polluted areas, i.e., northern China and YRD. Transportation of pollutants from these regions can have negative impacts on the local air quality of Hefei. Therefore, it is important to have an accurate estimation of the local emissions and transportation of pollutants, in order to have a better support in the future design of air quality related environmental policies. In this campaign, a mobile Multi-Axis Differential Optical Absorption Spectroscopy (MAX-DOAS) instrument was used to detect spatiotemporal distributions of NO₂. The resulting NO₂ vertical column densities (VCDs) are also used for the estimation of NO_x emission of Hefei. As the mobile MAX-DOAS observations provide valuable

information of the horizontal distribution NO₂, which cannot be resolved by the satellite observations with large footprint, the mobile MAX-DOAS results are also used to compare to satellite observations of the tropospheric NO₂ VCDs.

In this paper, we present a quantitative determination of the NO_x emission in Hefei using mobile MAX-DOAS measurements. In Section 2, detailed description of the measurement instrument, the data retrieval procedure as well as the introduction of other ancillary data is presented. An analysis of the spatial distribution of NO₂ over Hefei and the comparison to Ozone Monitoring Instrument (OMI) satellite observation is presented in Section 3.1. Section 3.2 presents the detailed error analysis of the NO_x emission calculation. The analysis of NO_x emission as well as the influence from local emission from regional transport of pollutants on local air quality is presented in Section 3.3.

2. Methodology

2.1. Mobile MAX-DOAS measurement

2.1.1. Experimental setup

In this study, a MAX-DOAS instrument was employed for mobile measurement in Hefei, China. The measurements were performed from 19 December 2016 to 19 February 2017. Details of the measurement schedule are listed in Table 3. During the mobile measurements, the MAX-DOAS instrument was setup on the top of a measurement vehicle at a height of 2 m above street level. The MAX-DOAS instrument consists of a scanning telescope, a stepping motor controlling the viewing elevation angle of the telescope and a spectrometer covering the wavelength range from 300 to 460 nm. Scattered sun-light collected by the telescope is redirected by a prism reflector and quartz fiber to the spectrometer for spectral analysis. The field of view of the instrument is about 0.5°. An Avantes spectrometer equipped with a Sony ILX554B-CCD silicon CCD detector was used. The Full Width Half Maximum (FWHM) spectral resolution of the spectrometer is 0.6 nm. An external laptop computer is used as controlling and data acquisition unit.

The viewing direction of the telescope was adjusted pointing along the measurement vehicle driving direction in order to avoid looking onto buildings on both sides of the road. A mobile measurement sequence consists of scattered sun-light measurement at elevation angles (α) of $1 \times 90^\circ$ (zenith), $2 \times 30^\circ$ (pointing toward the driving direction), $1 \times 90^\circ$ and $2 \times 150^\circ$ (pointing backward to the driving direction). In this study, both forward (30°) and backward (150°) measurements are used to avoid the influence of obstacles in the field of view of the telescope (buildings, trees, etc.) during the mobile measurement and result in a large measurement gap. In addition, this design also helps to reduce the influence of direction sunlight. In case of one of the measurement direction is blocked by a building or influenced by direct sunlight, the other measurement can still be used for retrieval. The total integration time of each measurement was set to 30 s with exposure time and number of scans adjusted automatically depending on the intensity of received scattered sun-light in order to achieve similar intensity levels for all the measurements. A full measurement sequence takes about 3 min. During the experiment, MAX-DOAS measurements were performed along a fix route along the Second Ring Road (inner route) and the Ring Expressway (outer route) of Hefei. The inner and outer route (blue and black) are indicated in Fig. 2. The blue line indicates measurement route taken in 2016 while the black line indicates measurement taken in 2017. The inner route surrounds the city center, while the outer route embraces of the entire urban area of Hefei. The positions of stationary MAX-DOAS (point C), in-situ monitor (point D), Luogang airport weather station (point E), Xinqiao airport (point A), and two power plants (point B and point F) are marked on Fig. 2. Measurement along the entire route (both inner and outer route) takes about 4 h depending on the traffic condition. A global positioning system (GPS) was used to record the geolocation information and the speed of the measurement vehicle.

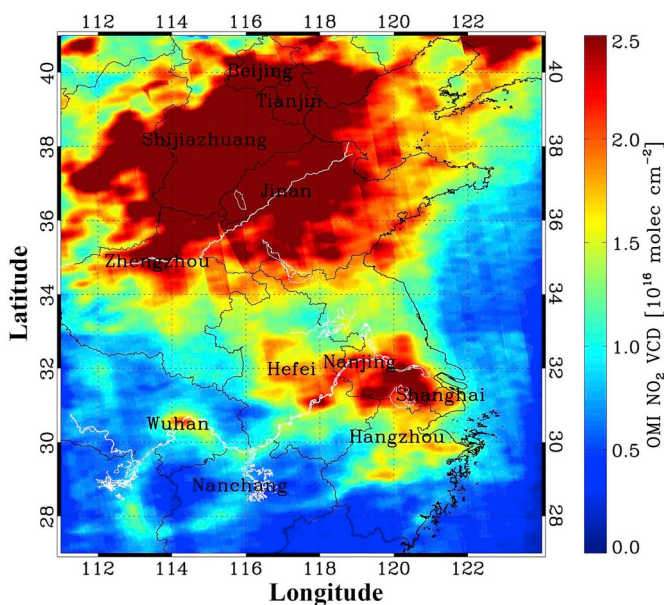


Fig. 1. The averaged OMI tropospheric NO₂ VCDs of winter time from December 2016 to February 2017 over eastern China.

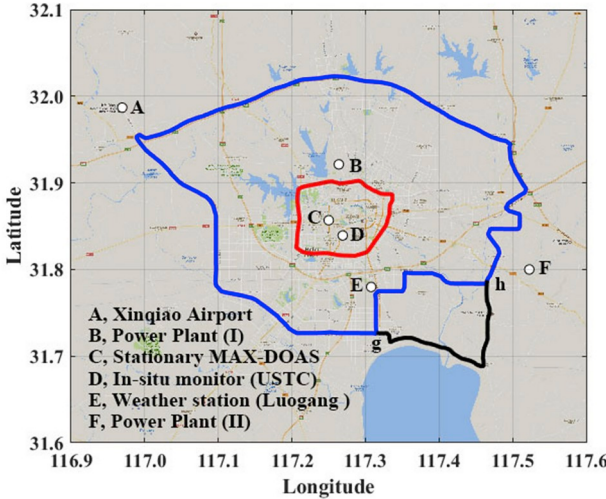


Fig. 2. The measurement routes taken during this campaign. The Second Ring Road (inner route) is indicated in red, and the Ring Expressway (outer router) is indicated in blue and black part. Major power plants, weather stations and our measurement instruments are marked on the figure. (For interpretation of the references to color in this figure legend, the reader is referred to the Web version of this article.)

2.1.2. Spectral retrieval

The DOAS technique was applied to analysis the measured spectra. All measured spectra were first corrected for offset and dark current. Subsequently, the off zenith measurement is divided by the corresponding zenith reference spectrum and taking the logarithm to convert to optical density. The DOAS fit is applied to wavelength range from 411 to 445 nm to retrieve the differential slant column densities (DSCDs) of NO₂. Broad band spectral structures caused by Rayleigh and Mie scattering are removed by including a 4th order polynomial in the DOAS fit. Absorption cross section of NO₂ at both 298 K and 220 K (Vandaele et al., 1998), O₄ at 293 K (Thalman and Volkamer, 2013), O₃ at 243 K (Serdychenko et al., 2014), H₂O at 296 K (Rothman et al., 2010) as well as the Ring spectrum were included in the spectral fitting analysis. Small shift and squeeze of the wavelength are allowed in the wavelength mapping process in order to compensate small uncertainties caused by the instability of the spectrograph. Wavelength and instrument slit function calibration achieved by fitting the measured zenith sky solar spectrum to the solar atlas (Chance and Kurucz, 2010). The resulting instrument function was used to convolve the literature reference cross sections to the instrument resolution. In this study, the spectra evaluation software QDOAS is used for the spectral fitting analysis (<http://uv-vis.aeronomie.be/software/QDOAS/>).

Data affected by direct sunlight, reflection from buildings and other objects are removed before the spectral analysis. In addition, measurements with root mean square (RMS) of DOAS fit residual larger than 0.005 are filtered.

2.1.3. Retrieval vertical column densities of NO₂

The measured NO₂ DSCDs were converted to VCDs using tropospheric differential air mass factors (DAMFs) according to the following formula:

$$VCD_{trop} = \frac{DSCD_{trop}}{DAMF} \quad (1)$$

$$DAMF = AMF_{\alpha \neq 90^\circ} - AMF_{\alpha=90^\circ} \quad (\alpha \text{ is the elevation angle of the telescope}) \quad (2)$$

Vertical distribution of aerosols and trace gases are important for the air mass factors (AMF) calculation. For the radiative transfer calculations, atmospheric profiles, i.e., pressure and temperature were taken from the Weather Research and Forecasting (WRF) model

simulations (see Section 2.3.1), while aerosol extinction and NO₂ profiles in the lowest 2 km of the troposphere were taken from the stationary MAX-DOAS (see Section 2.2.3) measurements. Aerosol and trace gas profiles above 2 km were obtained from WRF-Chem chemistry transport model simulations (see Section 2.3.2). Tropospheric AMFs of NO₂ were calculated at the central wavelength of the DOAS fitting windows (428 nm). Aerosol extinction profiles obtained from the stationary MAX-DOAS at 477 nm are converted to mobile MAX-DOAS retrieval wavelengths (428 nm) assuming a fix Ångström coefficient (Ångström, 1929) of 1. The aerosol extinction profiles at 428 nm can be derived using the following formula. Where z is the altitude and α is the Ångström coefficient.

$$\text{extinction}(428\text{nm}, z) = \text{extinction}(477\text{nm}, z) \times \left(\frac{428}{477} \right)^{-\alpha} \quad (3)$$

A fix set of single scattering albedo of 0.95, asymmetry parameter of 0.68 and surface albedo of 0.06 is assumed in the radiative transfer calculations. In this study, all AMF is calculated using radiative transfer model SCITRAN 2.2 (Rozanov et al., 2005). A more detailed description of the AMF calculation can be found in Hong et al. (2018).

2.2. Stationary MAX-DOAS

2.2.1. Experimental setup

A ground based MAX-DOAS instrument was setup on the roof of the Anhui Environmental Protection Bureau building which is located at the city center of Hefei (117.26°E, 31.85°N). The MAX-DOAS instrument consists of a telescope with a prism reflector, a stepping motor and a spectrometer. Scattered sun-light collected by the telescope is redirected by the prism reflector and the quartz fiber to the spectrometer for spectral analysis. The field of view of the instrument is less than 1°. Two spectrometers (Ocean Optic HR 2000 + and Maya2000Pro) were used to cover both the ultraviolet (UV, 303–370 nm) and visible (Vis, 390–608 nm) wavelength ranges. The FWHM spectral resolution of the UV and Vis spectrometers are 0.5 and 0.3 nm, respectively. The MAX-DOAS is controlled by a computer and operated automatically during the measurement.

A full measurement sequence consists of scattered sun light measurement at elevation angle of 1°, 2°, 3°, 4°, 5°, 8°, 10°, 15°, 30° and 90°(zenith) with azimuth viewing angle of 15°. The exposure time of each measurement is automatically adjusted depending on the intensity of the received scattered sunlight. The offset and dark current spectrum is taken by blocking the incoming light by a shutter. The offset and dark current spectrum is then automatically subtracted from the measured scattered sunlight spectra. A full measurement sequence takes about 5 min depending on the scattered sunlight intensity.

2.2.2. Spectral analysis

The stationary MAX-DOAS DSCDs are retrieved at two wavelength bands, which are 411–445 nm and 425–490 nm. The former band is used for NO₂ profile retrieval while the latter one is used to retrieve the aerosol extinction profile. Absorption cross section of NO₂, O₄, O₃, H₂O (Rothman et al., 2010; Serdyuchenko et al., 2014; Thalman and Volkamer, 2013; Vandaele et al., 1998) as well as the Ring spectrum were included in the spectral fitting analysis at 425–490 nm. The DOAS analysis settings for the 411–445 nm and is same as the mobile MAX-DOAS described in Section 2.1.2. Details of the DOAS fit settings are listed in Table 1.

2.2.3. NO₂ and aerosol profile retrievals

In this study, we use the HEIPRO algorithm (HEidelberg PROfile, developed by IUP Heidelberg) for aerosol and NO₂ profiles retrieval (Fries et al., 2006, 2011, 2016). As the radiative transfer equations cannot be linearized, the algorithm is fitting forward model results to observations to retrieve aerosol and NO₂ vertical distributions. The absorption signal of O₄ is used as the fitting quantity for the aerosol

Table 1
DOAS retrieval settings for mobile and stationary MAX-DOAS.

Parameter	NO ₂ (Stationary MAX-DOAS; Mobile MAX-DOAS)	O ₄ & NO ₂ (Stationary MAX-DOAS)	Reference
Fitting interval	411–445 nm	425–490 nm	
O ₄ (293 K)	✓	✓	Thalman and Volkamer (2013)
NO ₂ (298 K)	✓	✓	Vandaele et al. (1998)
NO ₂ (220 K)	✓	✓	10-correction (SCD of 10^{17} molec cm $^{-2}$) Vandaele et al. (1998)
O ₃ (223 K)	✓	✓	10-correction (SCD of 10^{17} molec cm $^{-2}$) Serdyuchenko et al. (2014)
H ₂ O ring	✓	✓	10-correction (SCD of 10^{20} molec cm $^{-2}$) HITEMP (Rothman et al., 2010)
Polynomial	Order 4	Order 5	Chance and Spurr (1997)

retrieval due to its well-known vertical distribution. The information contained in the MAX-DOAS observations is most likely not sufficient to retrieve an unique aerosol extinction profile. Therefore, the HEIPRO algorithm uses the Optimal Estimation Method (OEM, (Rodgers, 2000)) for the aerosol inversion. This approach supplemented the necessary information to the inversion in the form of a priori aerosol profile. In this study, a fix exponential decay a priori with aerosol optical depth of 0.32 and scale height of 1.0 km is used in the aerosol retrieval. The uncertainty of the aerosol a priori profile is set to 100% of the a priori extinction profile and the correlation length is set to 0.5 km in the retrieval. The lowest 3 km of the troposphere is divided into 15 layers, each with a height of 0.2 km. A fix set of single scattering albedo, asymmetry parameter and ground albedo is assumed in the aerosol retrieval which are 0.95, 0.68 and 0.06, respectively.

The aerosol information obtained from the procedure described above is converted to the NO₂ measurement wavelength of 428 nm using equation (3). The resulting aerosol extinction profiles are used for the differential box air mass factor (Δ DAMF) calculation for the NO₂ profile retrieval. The Δ DAMF was calculated at a single wavelength at 428 nm (center of the DOAS fitting range) and this Δ DAMF is assumed to be constant over the whole DOAS fitting window. Absorptions of trace gases are assumed to only have a negligible effect on the Δ DAMF calculation. As the NO₂ profile cannot be fully reconstructed by small number of MAX-DOAS observations, the HEIPRO algorithm uses the optimal estimation method to supply the necessary information as a priori to the NO₂ profile inversion. In this study, the NO₂ a priori profile is set to follow the exponential decay function with NO₂ VCD of 5.0×10^{15} molec cm $^{-2}$ and a scale height of 0.6 km. The error of the NO₂ a priori profile is set to 100% of the a priori and correlation length is set to 0.5 km. The atmosphere layer setting is same as the one used in the aerosol profile retrieval. The profile retrieval algorithm mentioned above is applied to the stationary MAX-DOAS measurements to retrieval both aerosol and NO₂ profiles during the mobile measurement campaign. The retrieved profiles are then used for air mass factor calculation for the mobile measurement to convert DSCDs to VCDs. In this study, retrieved profile with relative error larger than 50% and degree of freedom of signal (DFS) smaller than 2.0 are filter out. These criteria filtered 3.1% of all measurements.

2.3. Model simulation

2.3.1. Weather Research and Forecasting (WRF) model

The largest error in the estimation of the pollutant fluxes is caused by the uncertainty of the wind field. In order to obtain an accurate and high-resolution wind field data, WRF mesoscale meteorological model was used to downscale the global meteorological dataset (0.5° spatial resolution and 6-h time resolution) obtained from the National Center for Environmental Prediction (NCEP) Global Forecasting Model (GFS) to 1 km resolution for Hefei. Land surface characteristic is an important factor for the simulation of local wind fields. In order to reduce the

error caused by the land use database, high resolution land use data from MODIS was used in the simulation (Foy et al., 2006). The resulting wind field is in 1 km horizontal resolution with 34 vertical pressure sigma levels covering the entire Hefei city, which was used in NO_x emissions estimation (see Section 2.6). Meanwhile, the temperature and pressure profiles from the WRF model output were used to set up the atmosphere in RTM calculation described in Section 2.1.3.

2.3.2. WRF-chem simulation

WRF-Chem model simulation was performed to obtain reasonable aerosol extinction and NO₂ profiles above 2 km for the radiative transfer calculation (see Section 2.1.3), the spatio-temporal variation of NO_x to NO₂ ratios for the NO_x emission sensitivity analysis (see Section 3.2.5), and the NO₂ and atmospheric profiles used in the AMFs calculation for satellite retrieval (see Section 2.4). In this study, the WRF-Chem model (version 3.7) is used to simulate the 3-dimensional distributions of atmospheric pollutants. The model domain was adjusted to cover the Eastern China and its surrounding areas, with a grid resolution of 20 × 20 km and 26 vertical layers. The model setup is similar to the setup described in Liu et al. (2016b) and Su et al. (2017). The NCEP (1° spatial resolution and 6-h time resolution) were used as the initial and boundary conditions for meteorological field simulation. The Carbon-Bond Mechanism version Z (CBMZ) photochemical mechanism is combined with the Model for Simulating Aerosol Interactions and Chemistry (MOSAIC) aerosol model for the simulation of chemical process in the atmosphere. The anthropogenic emission inputs were taken from the Multi-resolution Emission Inventory for China (MEIC, <http://www.meicmodel.org/>).

2.4. Satellite observations

Ozone Monitoring Instrument (OMI) is an imaging spectrometer onboard the NASA Earth Observing System (EOS) Aura satellite which was launched in 2004 (Levitt et al., 2006). It measures solar spectra reflected from the Earth. The spectral range of OMI covers both UV and visible band from 270–500 nm, which allow the retrieval of ozone, NO₂, and other trace gases. Local equator overpass time of OMI is 13:45 on the ascending node.

In this study, the USTC's OMI tropospheric NO₂ product is used. The product has been reported to be more representative over China as it uses better NO₂ a priori profiles in the air mass factor calculation (Hong et al., 2018; Liu et al., 2016b; Su et al., 2017; Tan et al., 2018; Xing et al., 2017). Slant Column Densities (SCDs) of NO₂ are retrieved by applying the DOAS fit to OMI spectra. Separation of stratospheric and tropospheric columns is achieved by the local analysis of the stratospheric field over unpolluted areas (Bucsela et al., 2013; Krotkov et al., 2017). The OMI NO₂ SCDs are converted to VCDs by using the concept of AMF. The AMFs are calculated based on the NO₂ and atmospheric profiles derived from WRF-Chem chemistry transport model simulations with a horizontal resolution of 20 × 20 km over eastern China.

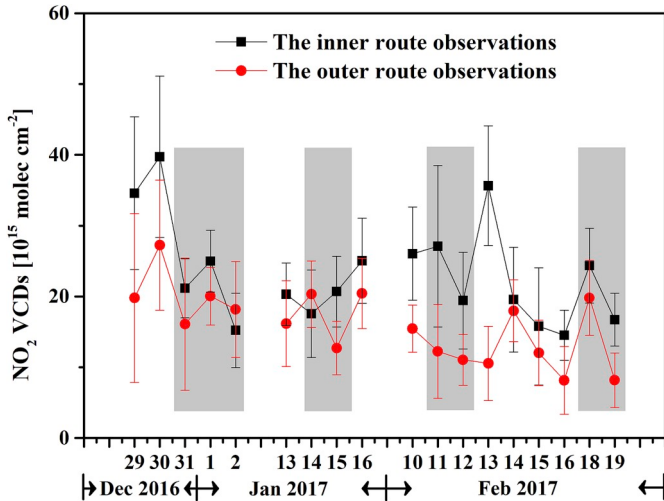


Fig. 3. Time series of averaged NO₂ VCDs measured by the mobile MAX-DOAS along the inner route (black curve) and the outer route (red curve) during this campaign. Weekends and holiday are indicated by the grey shadow. (For interpretation of the references to color in this figure legend, the reader is referred to the Web version of this article.)

2.5. Ancillary data

Meteorological parameters (wind direction and wind speed information) were obtained from an automatic weather station located at Luogang airport in Hefei (point E in Fig. 2 and 117.31°E, 31.78°N). The measured wind information was used to validate the WRF model simulations wind results at the height of 10 m. In addition, NO and NO₂ data are obtained from an in-situ NO–NO₂–NO_x analyzer (Thermo, model 42i) installed on the roof of the first academic buildings of USTC (point D in Fig. 2 and 117.27°E, 31.84°N). The data are used to calculate the NO_x/NO₂ ratio during the mobile measurement campaign.

2.6. Determination of the NO_x emissions

Mobile measurements were performed to quantify the transportation as well as the emission source strength of air pollutants in Hefei. With the supplementary of meteorological information, NO₂ flux can be calculated using the following equation (Ibrahim et al., 2010):

$$\text{Flux}_{\text{NO}_2} = \oint VCD(s) \cdot \vec{\omega} \cdot \vec{n} \cdot ds \quad (4)$$

As the measurements is discretized, and implemented in segments, the NO₂ flux can be estimated by the sum:

$$\text{Flux}_{\text{NO}_2} \approx \sum VCD_{\text{NO}_2}(S_i) \cdot \omega_i \cdot \sin(\beta_i) \cdot \Delta S_i \quad (5)$$

Where VCD indicates the averaged NO₂ vertical column density measured by the mobile MAX-DOAS, ω represents the wind speed of the observation place, β indicates the included angle between wind direction and the driving direction, and ΔS is the distance between two success measurements.

In this study, geolocation information is recorded using a GPS sensor on board the measurement vehicle. The hourly wind data with 1 × 1 km resolution obtained from WRF simulation (see Section 2.3.1) is interpolated in both spatial and temporal dimension to the mobile MAX-DOAS measurement resolution. Height resolved wind field data are then combined with the mobile MAX-DOAS VCDs for flux calculation.

As wind speed, wind direction and NO₂ concentration strongly vary with altitude, using an averaged wind data for the emission flux estimation would result in large errors. On the other hand, the stationary MAX-DOAS provides vertical distribution information of atmospheric NO₂. Assuming the vertical profile measured by the stationary MAX-

DOAS is representative for the entire Hefei, we average the wind field data by using the stationary MAX-DOAS NO₂ vertical profile as weighting following equation:

$$v_{\text{ave}} = \sum_i v_i \cdot w_i \quad (6)$$

Where v_i indicates the wind vector at height layer i and w_i indicates the weight at the layer i.

Although the retrieval height of the MAX-DOAS is set to 3 km, however, the sensitivity above 2 km is rather low. In addition, the mixing layer height in Hefei during winter is usually below 2 km. Therefore, we only use the NO₂ profiles retrieved from the stationary MAX-DOAS observations at the lowest 2 km with the upper part replaced by the WRF-chem simulated profiles. Both the mobile and stationary MAX-DOAS only provide NO₂ observations. In order to estimate the flux of total NO_x, the in-situ measurement of NO and NO₂ is used to calculation the NO_x/NO₂ratios (C_L) for the conversion of NO₂data to total NO_x. Another important factor for flux estimation is the lifetime correction (C_τ) of NO_x emissions, which is dependent on the atmospheric lifetime of NO_x τ , wind speed ω and distance between emission source and measurement location D. NO_x emission flux can be determine using equation (7) while the lifetime correction coefficient of NO_x defined by equation (8).

$$\text{Flux}_{\text{NO}_x} = C_L \cdot C_\tau \cdot \text{Flux}_{\text{NO}_2} \quad (7)$$

$$C_\tau = e^{\frac{t}{\tau}} = e^{\frac{D/\omega}{\tau}} \quad (8)$$

Typically urban NO_x has a lifetime of 6 h during day time in winter (Beirle et al., 2011; Ibrahim et al., 2010). Details of the calculation and uncertainties estimation of the lifetime correction factor is described in Section 3.2.4.

3. Results and discussion

3.1. NO₂ VCDs results

3.1.1. Distribution of NO₂ VCDs

NO₂ VCDs along the measurement routes are used to analysis the spatiotemporal distribution of NO₂ in Hefei. Fig. 3 shows the daily averaged NO₂ VCDs time series for both inner and outer routes. Measured NO₂ VCDs vary from $(14.51 \pm 3.54) \times 10^{15}$ to $(52.14 \pm 16.65) \times 10^{15}$ molec cm⁻² along the inner route (black curve), with a mean value of $(24.76 \pm 9.70) \times 10^{15}$ molec cm⁻², while the NO₂ VCDs measured along the outer route vary from $(8.51 \pm 4.78) \times 10^{15}$ to $(28.15 \pm 23.74) \times 10^{15}$ molec cm⁻² (red curve), with an average value of $(16.55 \pm 5.67) \times 10^{15}$ molec cm⁻² during the campaign. As most of the emissions (such as industry, power, residential and transportation emissions) are concentrated close to the city center, the NO₂concentration is over the inner route is in general higher than the outer route by a factor of 1.50. An example of the NO₂distribution observed on 29 December 2016 along both measurement route is shown in Fig. 4, the averaged NO₂ VCD along the inner route is $(35.01 \pm 10.73) \times 10^{15}$ molec cm⁻² while the average over the outer route is dropped to $(20.28 \pm 12.72) \times 10^{15}$ molec cm⁻². However, higher NO₂ VCDs were measured along the outer route on 2 and 14 January 2017 compared to the inner route. This can be explained by emissions reduced in city center and higher traffic emissions along the outer route. As these two days are holidays, therefore, people are likely to travel home or make a short trip outside the city, resulting in higher traffic in the suburban. Moreover, the diurnal variation pattern of NO₂ is another factor influencing the measurement results. The diurnal pattern of NO₂ in weekend is slightly different from that of weekdays. The morning rush hour peak is delayed and extended for a longer time during weekend. In addition, the inner route measurement was taken in the morning and the outer route measurement

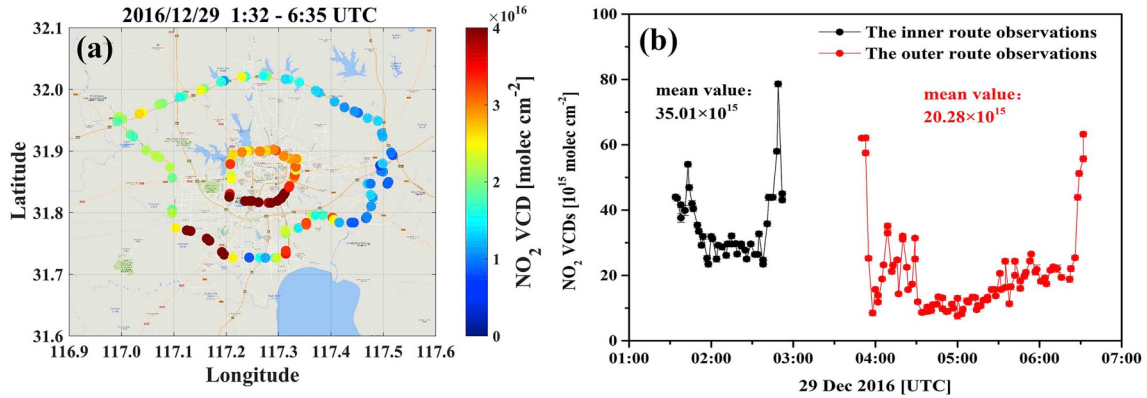


Fig. 4. NO₂ VCDs measured on 29 December 2016; (a) the spatial distribution of NO₂ VCDs, and (b) the time series of NO₂ VCDs along the inner route (black curve) and outer route (red curve). (For interpretation of the references to color in this figure legend, the reader is referred to the Web version of this article.)

was taken in the late morning and early afternoon. This also explain the phenomenon that the NO₂ VCDs detected along the outer route were higher for some measurement days.

Variations of NO₂ VCDs are closely related to the variation of emission sources and meteorological conditions (e.g., wind speed and wind direction). Mobile measurement results in general show higher NO₂ values over the downwind side (see Fig. 5). The averaged NO₂ VCD over downwind area of the outer route during the entire campaign is $(18.69 \pm 8.04) \times 10^{15}$ molec cm⁻², while it is $(14.27 \pm 5.62) \times 10^{15}$ molec cm⁻² for upwind areas. However, the NO₂ VCDs over upwind areas are higher than the downwind side during some measurement days. This is mainly due to the higher emissions over the upwind areas and regional transport of pollutants. On 30 December 2016 and 14 January 2017 (see Fig. 8b), easterly wind brought the emissions from the power plant (point F in Fig. 2) into the city and resulted in higher NO₂ VCDs over the upwind area. On the other hand, measurements taken on 13 January 2017 were seriously influenced by surroundings especially the pollutants transport from the north.

We have also examined the so-called “holiday effects” using the mobile measurement of NO₂. The mobile measurements were performed continuously from 29 December 2016 to 2 January 2017, covering the New YearEve and New Year holiday. We observed a significant reduction of NO₂ VCDs (~45%) during the New Year holiday, the averaged NO₂ VCD along the inner route decreased from

$(37.16 \pm 3.65) \times 10^{15}$ molec cm⁻² on 30 December 2016 to $(20.45 \pm 4.93) \times 10^{15}$ molec cm⁻² on 31 December 2016. Similar reduction of NO₂ VCD can also be observed over the outer routes, NO₂ VCDs reduced from $(23.52 \pm 5.28) \times 10^{15}$ molec cm⁻² to $(18.10 \pm 1.98) \times 10^{15}$ molec cm⁻². We have also looked into the weekend effect for measurement from 13 January to 19 February, 2017. In general, we observed a ~13% lower NO₂ VCDs along the inner route on Sunday ($(18.94 \pm 2.02) \times 10^{15}$ molec cm⁻²) compared to weekdays ($(21.59 \pm 7.08) \times 10^{15}$ molec cm⁻²). A more significant weekend reduction (~28%) is also observed over the outer route with averaged NO₂ VCDs of $(14.58 \pm 4.05) \times 10^{15}$ molec cm⁻² and $(10.64 \pm 2.30) \times 10^{15}$ molec cm⁻² for weekdays and Sundays, respectively. This phenomenon can be explained by the different characteristic of land use. The major NO_x emission sources in urban area are traffic emissions. Most of the commercial areas are concentrated in the city center, while residential buildings are mostly located outside of the inner route. As the commercial areas are usually operated 7 days a week in China, while large portion of people do not have to work during weekend. Therefore, the weekend reduction effect is more significant over residential areas outside the inner route compared to the city center.

3.1.2. Comparison of stationary and mobile MAX-DOAS

In order to investigate how representative the stationary MAX-DOAS measurement for the entire city, we compared daily average mobile measurement of NO₂ VCDs to the stationary MAX-DOAS. Fig. 6a shows the time series of daily averaged NO₂ VCDs measured by the mobile MAX-DOAS along the inner route and stationary MAX-DOAS averaged during the inner route measurements. Fig. 6b shows the comparison of daily averaged NO₂ VCDs between mobile MAX-DOAS inner route measurements and stationary MAX-DOAS. Fig. 6c and d are same as Fig. 6a and Fig. 6b but for measurements along the outer route. Mobile measurements along the inner route show a better agreement to the stationary MAX-DOAS observations compared to measurements taken along the outer route. The temporal development of the mobile measurement of NO₂ VCDs along the inner route agrees well with the stationary MAX-DOAS observations with a Pearson correlation coefficient (R) of 0.77. The overall average NO₂ VCDs measured by the mobile MAX-DOAS along the inner route is 25.41×10^{15} molec cm⁻² while the stationary MAX-DOAS reports an average NO₂ VCDs of 24.19×10^{15} molec cm⁻² during the same period. A lower averaged NO₂ VCD of 18.03×10^{15} molec cm⁻² is reported from measurement along the outer route, while the averaged NO₂ VCD measured by the stationary MAX-DOAS is 25.37×10^{15} molec cm⁻² during the same time. The Pearson correlation coefficient (R) between the two datasets reduced to 0.62. The correlation reduced with increasing distances between the two instruments. The result indicates the strong spatial gradient of NO₂ over the city. Higher NO₂ VCDs measured over the city

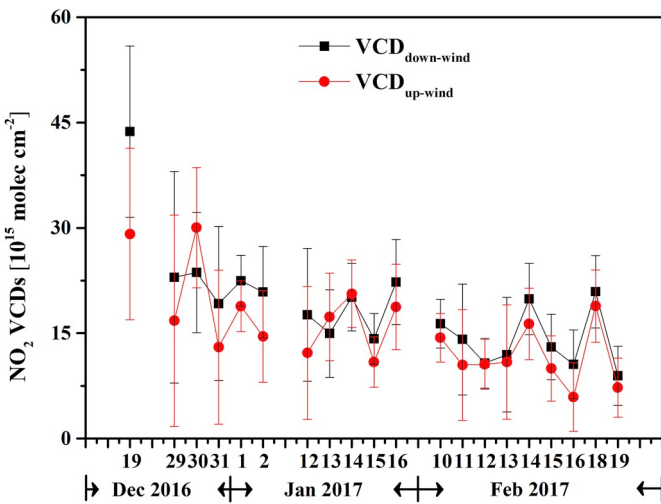


Fig. 5. Time series of daily averaged NO₂ VCDs over upwind (red curve) and downwind (black curve) areas of the outer route. (For interpretation of the references to color in this figure legend, the reader is referred to the Web version of this article.)

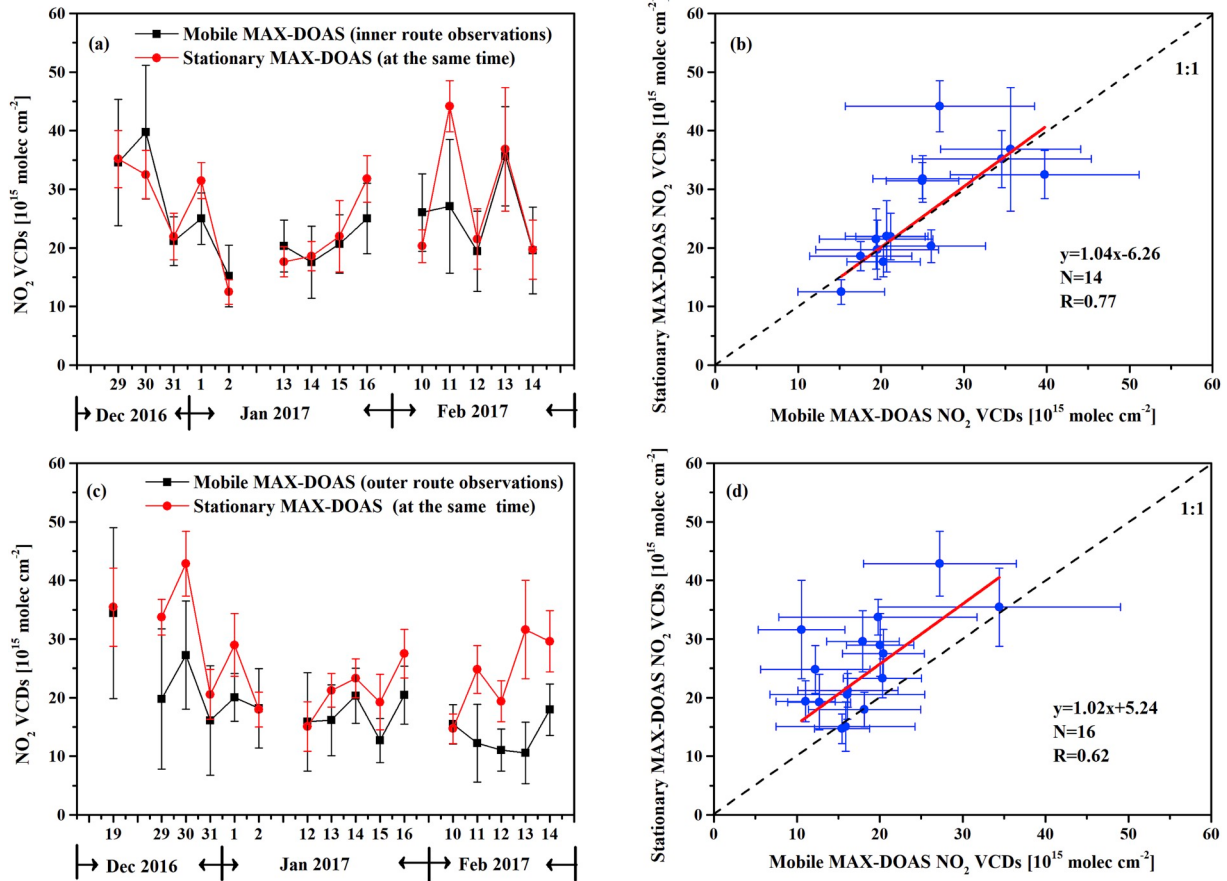


Fig. 6. Time series of daily averaged tropospheric NO₂ VCDs measured by stationary MAX-DOAS and mobile MAX-DOAS along (a) the inner route and (c) the outer route. Comparison of daily averaged NO₂ VCD between stationary MAX-DOAS and mobile measurement along inner route and outer route are show in (b) and (d), respectively.

center also implies that the emissions of NO₂ are more concentrated at the city. As NO₂ VCDs measured by both mobile and stationary MAX-DOAS agree with each other, we assumed that the NO₂ vertical profiles measured by the stationary MAX-DOAS are representative for the city and can be used to improve the emission estimation from mobile measurements.

3.1.3. Comparison of MAX-DOAS and OMI NO₂ VCDs

In this study, mobile MAX-DOAS measurements of NO₂VCDs are compared to OMI satellite observations. Time series of tropospheric NO₂

VCDs measured by OMI satellite over Hefei and the mobile MAX-DOAS observations are shown in Fig. 7a. A scatter plot between the two dataset is also shown in Fig. 7b. OMI observations are spatially averaged over Hefei (116.8°E–117.8°E, 31.3°N–32.3°N) while mobile MAX-DOAS measurements are spatiotemporally averaged along the outer route measurement route. Satellite data with cloud radiance fraction larger than 0.4 is considered as cloud contaminated and it is not used in the comparison. In total, there are 10 valid measurement days for the comparison. NASA's OMI NO₂ VCDs are also shown for reference. As shown in Fig. 7, USTC's OMI tropospheric NO₂ VCDs show a better

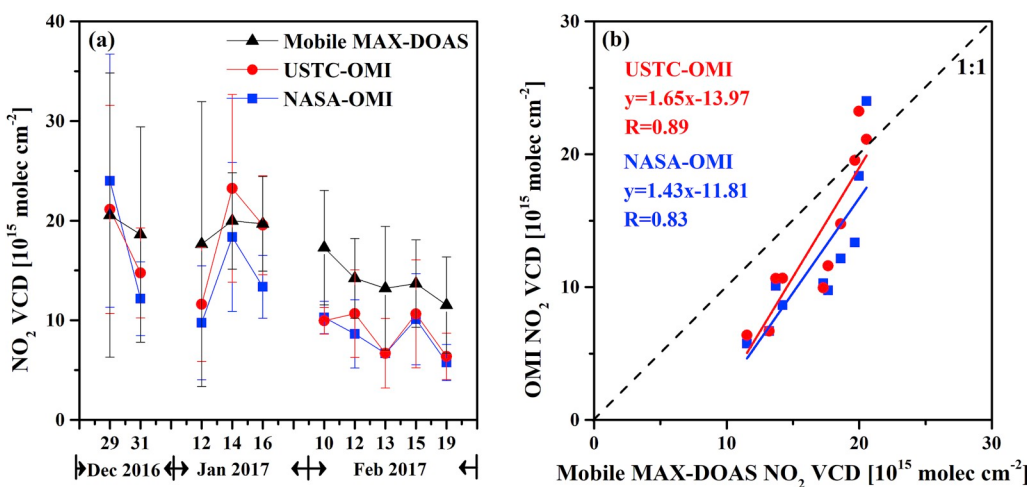


Fig. 7. Comparison of daily averaged tropospheric NO₂ VCDs measured by mobile MAX-DOAS (black markers) along the outer route, USTC's (red markers) and NASA standard (blue markers) OMI product over Hefei (116.8°E–117.8°E, 31.3°N–32.3°N), (a) the time series and (b) the correlation analysis. (For interpretation of the references to color in this figure legend, the reader is referred to the Web version of this article.)

agreement to the mobile measurements compared to the NASA's standard product. The Pearson correlation coefficient (R) between the mobile measurement and USTC product is 0.89 while the correlation reduced to 0.83 when comparing to the NASA's standard product. Both satellite data sets underestimated the tropospheric NO_2 VCD by about 19–28% on average. Compared to the NASA standard OMI product, the USTC's OMI tropospheric NO_2 product uses the NO_2 profiles derived from WRF-Chem chemistry transport model simulations as a priori profile. The spatial resolution of the WRF-Chem simulation is higher than the one used in the standard product and therefore shows a better agreement with ground measurements. In addition, the USTC tropospheric NO_2 product shows a smaller bias compared to the NASA standard product. The discrepancies can be explained by the uncertainties in the air mass factor calculations related to the aerosols and NO_2 vertical distribution profiles used in the OMI retrieval. Differences in the spatial coverage of the MAX-DOAS and OMI measurements also contribute to the discrepancies. In addition, differences in measurement time also contribute to the discrepancies between two datasets. Mobile MAX-DOAS measurements were performed between 9:00 to 16:00 Local Time (LT) while the OMI overpass time is around 13:45 LT. Due to stronger photolysis at noon time, the NO_2 concentration is expected to be lower. We have also compared daily averaged NO_2 VCDs measured along the inner route with the OMI observations. However, the agreement is much worse than the outer route measurements. The result implies that satellite observation with low spatial resolution is not capable to capture the spatial variation of NO_2 over pollution hotspots.

In order to investigate the spatial distribution of tropospheric NO_2 , mobile MAX-DOAS measurements are plotted together with OMI observations for 4 measurement days which are shown in Fig. 8. The different days observations are marked in the title of Fig. 8a, (b), (c) and (d), the zoom of Hefei area on the left is corresponding to the black rectangle on the right and the backward trajectories at different height were colored in different kinds of colors in Fig. 8. OMI tropospheric NO_2 VCDs are gridded with a resolution of $0.01^\circ \times 0.01^\circ$ using the parabolic spline gridding algorithm (Chan et al., 2015, 2017; Kuhlmann et al., 2014). The two datasets in general agree well with each other. Backward trajectories of air masses simulated by the HYSPLIT model (Stein et al., 2016) are used to assess the transportation of atmospheric NO_2 during the measurement campaign. The backward trajectories are calculated at the stationary MAX-DOAS site (117.26°E , 31.85°N) with height of 200 m (Su et al.), 400 m (blue) and 800 m (white) above ground level. OMI satellite observations show a relatively high NO_2 VCDs over Hefei compared to surrounding areas. However, the absolute values are far lower than that of the northern China and YRD. The backward trajectory analysis of these four cases shows that the air quality in Hefei was significantly influenced by air mass transportation from the north (i.e., on 29 December 2016, 10 February 2017) and the east (i.e., on 14 and 16 January 2017) in winter.

3.2. Sensitivity and error analysis

The calculation of NO_x emission from mobile MAX-DOAS measurements can be influenced by several factors. In this section, we present the sensitivity analysis of NO_x emission estimation to different factors to identify the major sources of errors and their impact on the emission calculation.

3.2.1. Errors caused by NO_2 VCDs

The NO_2 DSCDs were retrieved by applying the DOAS technique to the measurement spectra. Error of DSCDs can be estimated through the analysis of the DOAS residual. As the absorption signal of NO_2 over urban area is rather strong, the DOAS fitting errors of the NO_2 DSCDs is insignificant compared to other sources of error. One of the largest uncertainties comes from the conversion of NO_2 DSCDs to VCDs. In this study, NO_2 DSCDs measured by the mobile MAX-DOAS were converted to VCDs using air mass factor calculated by RTM. The calculation of

AMF using RTM is expected to be more accurate than the geometric approximation as it also considers the influences from viewing geometry, aerosol and NO_2 profiles. However, all of these inputs is associated with uncertainties and the uncertainties of aerosol and trace gases profiles dominated the error in the AMF calculations. In this study, the aerosol extinction and NO_2 profiles are obtained from the stationary MAX-DOAS. The retrieval error of the aerosol optical depth (AOD) is on average 8.5% during the measurement campaign, while the mean value of NO_2 VCD error is 1.5%. A sensitivity study was performed to examine the influence of aerosol and NO_2 profile uncertainty on the AMF calculation. We scaled the retrieved aerosol extinction profiles by $\pm 8.5\%$, $\pm 17\%$ and $\pm 25.5\%$ for the sensitivity study. The scaled aerosol extinction profiles were then used in the RTM simulation for the AMF calculations. The result shows that the AMF is on average 0.9%, 1.0% and 1.1% different from the one calculated using the original aerosol profile. The uncertainty caused by NO_2 profile was estimated by taking different profile shape into account. Four scenarios were considered in the sensitivity analysis, 1) simultaneous NO_2 profile measured by the stationary MAX-DOAS, 2) averaged NO_2 profile measured during the entire campaign, 3) NO_2 profile with lowest NO_2 VCD measured during the campaign and 4) NO_2 profile with highest NO_2 VCD measured during the campaign. The result shows the AMF varies by $\pm 7.3\%$ for these 4 scenarios. This variation of the AMF is considered as the uncertainty related to the error of NO_2 profile. Taking both aerosol and NO_2 uncertainty into account, the total NO_2 VCD error is estimated as 7.4%. Our estimation of VCD error agrees with previous similar studies (Hong et al., 2018; Wu et al., 2013). As this is only a rough estimation and the aerosol and NO_2 profiles could vary in a wider range. Therefore, we use a rather conservative percentage error of 10% in this study to avoid underestimation of the error.

3.2.2. Errors caused by measurement gaps

The mobile measurement of NO_2 VCDs are discretized, each measurement represents the intensity weighted average VCD along the measurement route traveled within the measurement time. The total flux of NO_2 is determined by discretized measurement segments (Eq. (5)) instead of continuous observations (Eq. (4)). As a measurement cycle contains zenith measurement which is used as reference and not evaluated in the analysis. In addition, some measurements are blocked by buildings, influenced by cloud or interrupted due power problem of the measurement vehicle. Therefore, there might be areas without valid measurement. The distance between two valid measurements is considered as measurement gap, for instance, power problem caused a large gap of ~ 15 km on 19 December 2016 (see Fig. 9). Large measurement gaps can lead to large uncertainties in the emission results. Most of the mobile measurement studies show that measurements gap is one of the major sources of error. To determine the errors caused by measurement gaps, we assume a rather complete measurement route as the ground truth and artificially remove some data to examine the effect of missing data. Two scenarios were tested. The first scenario, we separated the 150 km measurement route into 30 segments with each segment of 5 km, while the second scenario separates the measurement route into 15 segments with the distance of each segment of 10 km. The NO_2 emission flux is calculated with measurements within one of these segments removed. The emission calculated is compared to the estimation with the complete measurement (no data is removed). We consider the difference as the error induced by measurement gap. This calculation is then repeated for each of these segments. The uncertainty can be estimated by analyzing the statistic of the difference between the complete cycle and the one with data removed. The result shows the error caused by measurement gap of 5 km is about $(20.6 \pm 18.2)\%$ while measurement gap of 10 km would introduce an error of $(38.9 \pm 29.1)\%$. As the error increases with the distance of gap and 10 km of measurement gap already result in a significant error, we do not consider measurement days with measurement gap larger than 10 km (listed in Table 3) in the emission calculation. The error induced

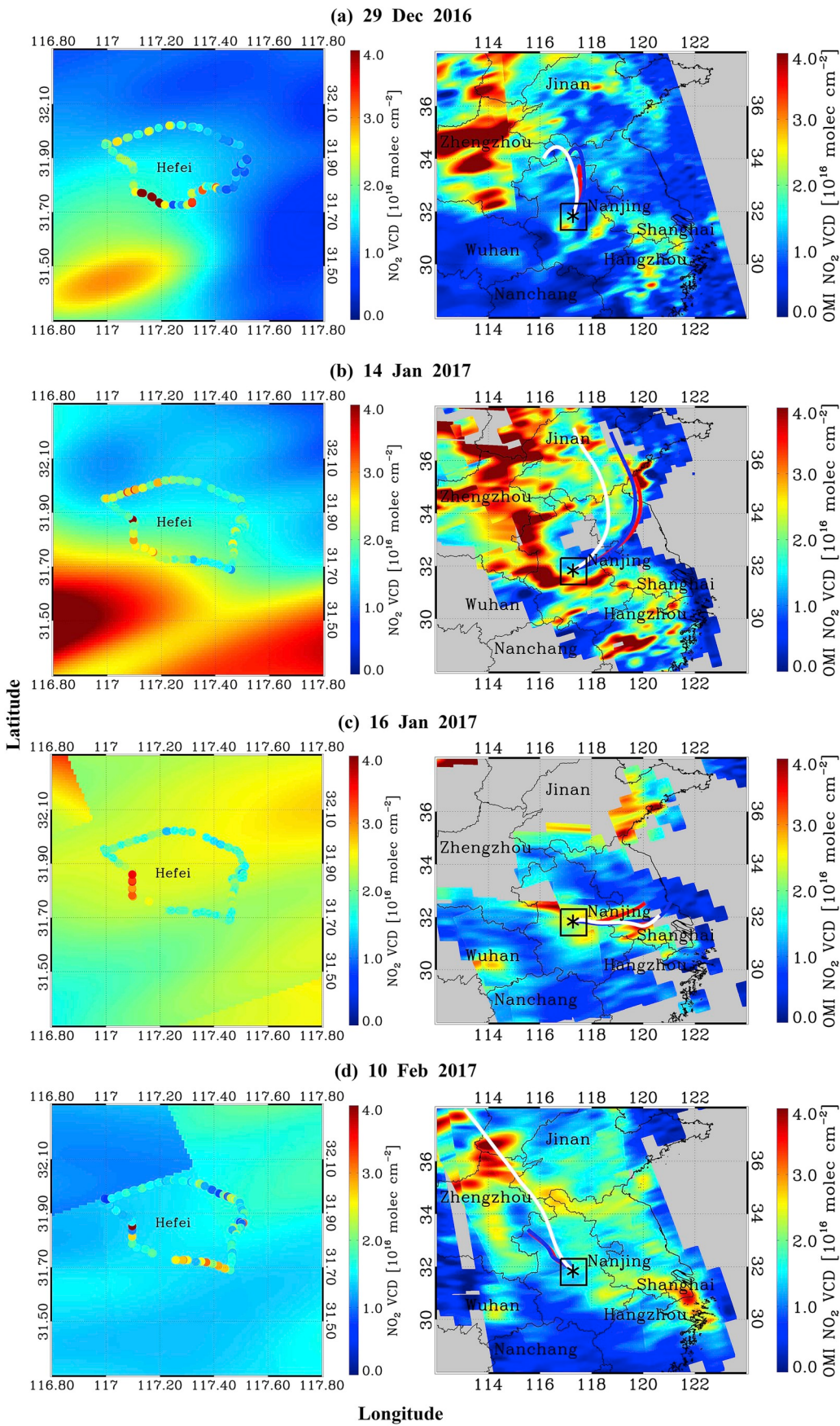


Fig. 8. Spatial distribution of tropospheric NO₂ VCDs measured by both mobile MAXDOAS and OMI satellite of (a) 29 Dec 2016, (b) 14 Jan 2017, (c) 16 Jan 2017 and (d) 10 Feb 2017. Zoom in maps of Hefei are shown in the left panels, while the right panels show the entire eastern China. Backward trajectories of air masses are also shown to illustrate the transportation of atmospheric NO₂ during the measurement campaign, the red, blue and white lines indicate the 24 h backward trajectories at the height of 200 m, 400 m and 800 m above ground level, respectively. (For interpretation of the references to color in this figure legend, the reader is referred to the Web version of this article.)

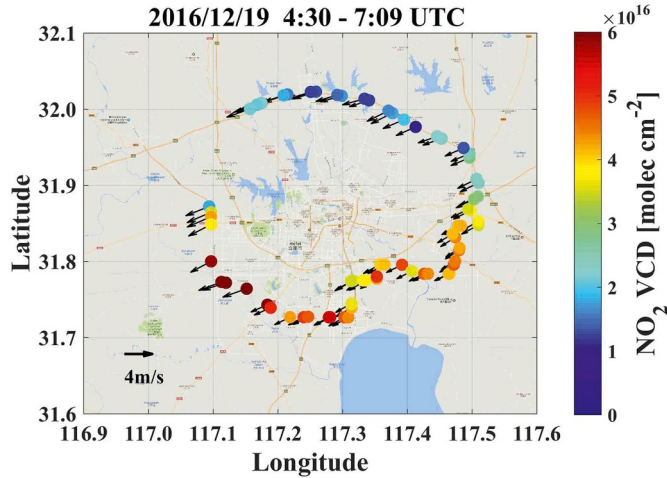


Fig. 9. An example mobile MAX-DOAS measurement on 19 December 2016. The measurement gap (~ 15 km) is caused by power failure of the measurement vehicle.

by measurement gap for each day is estimated following the approach mentioned above. The measurement route is separated into certain segments, each with a distance equal to the measurement gap of the day. We then compare the emission calculated with data within each of these segments removed to the complete cycle to estimate the uncertainty caused by measurement gap for each day. According to our estimation, the error caused by measurement gap is ranging from 13.1% to 34.7% with an average value of 20.1% during our measurement campaign.

3.2.3. Errors caused by wind data

Wind data is an important factor for the NO_x emission estimation. The uncertainty of wind data could result in a significant error in the emission estimation. As it is difficult to have a 3-dimensional wind field measurement, therefore, wind data used in this study is taken from the WRF model simulation. The wind data is interpolated in both spatial and temporal dimension to the mobile measurement time and location. In order to examine the accuracy of the modeled wind field, we compared the wind speed and wind direction taken from the WRF

simulations and the wind measurements from the meteorological station at Luogang airport. **Fig. 10** shows the time series of wind direction and wind speed at 10 m (above ground level) from WRF simulations and meteorological station observations at Luogang airport from 19 December 2016 to 19 February 2017. Hourly data are presented. The results show that the modeled wind data in general agrees well with the meteorological station observations. As measurements were performed during daytime, we compared the model data to observations from 9:00 to 15:00 local time (most of the measurements were taken within this period) of all measurements. The averaged absolute difference of wind speed is 0.81 m s^{-1} , while the averaged absolute difference of wind direction is 18.06° . We assumed the wind speed and wind direction errors are constant during our measurements. Taking wind speed error into account in the emission calculation would result in an error of 5.7%–26.9% of the NO_x emission with a mean value of 16.5%, while the wind direction error would cause an error of 4.9%–54.2% with a mean value of 21.0%. The total error caused by wind speed and wind direction can be calculated by error propagation equation. The resulting uncertainty of NO_x emissions caused by wind varies from 8.8% to 54.5% with mean value of 32.2%. As low wind speed and large variation of wind direction would result in large uncertainty in the emission approximation, therefore, we excluded measurement days with averaged wind speed below 2 m s^{-1} and wind direction variation large than 30° in our analysis.

3.2.4. Errors caused by NO_x lifetime correction

The approximation of NO_x lifetime in the atmosphere has a significant impact on the NO_x emission calculation. The NO_x lifetime is strongly dependent on meteorological parameters (e.g. temperature), photolysis rate and abundance of other reactive trace species in the atmosphere. Therefore, it is difficult to have an accurate approximation. In this study, we assume a NO_x lifetime of 6 h which has been reported to be realistic in winter (Beirle et al., 2011; Ibrahim et al., 2010). The length of the outer measurement route is about 150 km and the average distance to the city center (stationary MAX-DOAS site) is about 20 km. Combining with wind information, the lifetime correction factors (C_r) can be obtained using equation (8). In this study, we filter data with wind speed lower than 2 m s^{-1} (with respect to lifetime correction factor of 1.6) in order to avoid large error in the emission estimation. After removed invalid data, the lifetime correction factor varies from 1.07 to 1.53 (listed in Table 4) with an average of 1.26 during the

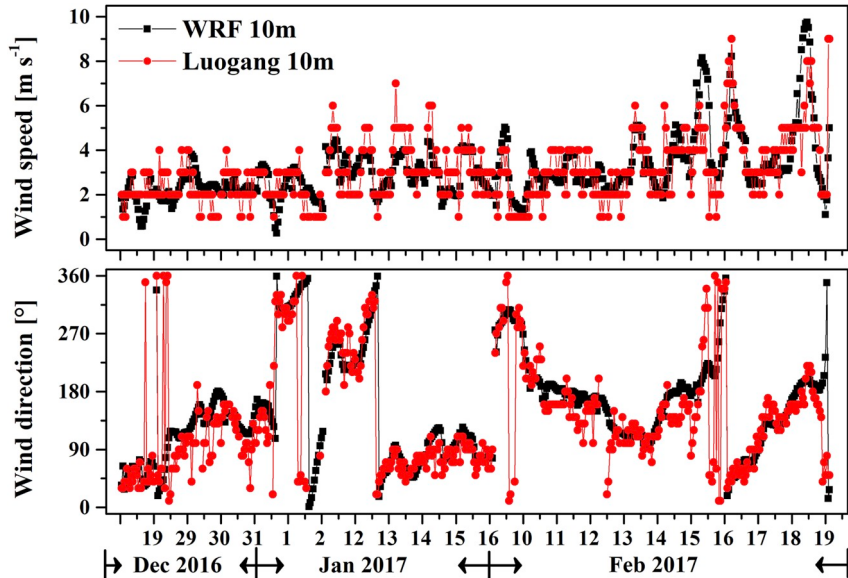


Fig. 10. Time series of wind direction and wind speed simulated by WRF (black curve) and measured by the weather station at Luogang airport (red curve) in Hefei. (For interpretation of the references to color in this figure legend, the reader is referred to the Web version of this article.)

campaign. Owing the assumption of NO_x life time of 6 h is a rough approximation and could deviate from the assumed value on different days. This assumption would result in additional error in the emission calculation. In order to determinate the uncertainties caused by NO_x lifetime, we assume the error of NO_x lifetime is about 2 h which is realistic according to previous NO_x lifetime study (Lin et al., 2010; Liu et al., 2016a). Taking this into account in the calculation would result in an uncertainty of 2.4%–16.9% in the NO_x emission with an average value of 8.7%.

3.2.5. Errors caused by NO_x/NO₂ ratio

The atmospheric NO_x/NO₂ratio (C_L) is highly dependent on meteorological conditions (e.g., solar irradiance) and other trace species in the atmosphere (e.g., O₃). In addition, the NO_x/NO₂ ratio also shows a strong spatial variability due different characteristic of pollution sources. For example, the contribution of NO to total NO_x level can be very high for area close to large emission sources, e.g., power plant. In these cases, the total NO_x emission can be significantly underestimated.

In this study, daily averaged NO_x/NO₂ ratios used in the calculation of total NO_x emission are taken from an in-situ monitor located on the roof of the university building. The measurement data were temporally averaged within the mobile measurement period of the day. The resulting NO_x/NO₂ ratio varies from 1.06 to 1.89 with a mean value of 1.28 (listed in Table 4), which is similar to the ratio of 1.32 assumed in previous study (Shaiganfar et al., 2011). As the mobile measurement usually takes several hours and the atmospheric NO_x/NO₂ could vary in a wide range during the measurement, using an average NO_x/NO₂ ratio would result in a significant uncertainty in the total NO_x emission calculation. In addition, the in-situ measurement might not be fully representative for the entire city. On the other hand, model simulation also provides information of the NO_x/NO₂ ratio for the entire city. We compared the spatial and temporal interpolated model simulation of NO_x/NO₂ ratio to the in-situ measurements. The result shows good agreement with each other with Pearson correlation coefficient (R) of 0.94. However, the spatial average of modeled NO_x/NO₂ ratio over the entire city shows higher ratio of 1.29–2.31 with mean value of 1.60. As the NO_x/NO₂ratios obtained from model simulation seem to be too high (~1.25 times of the measurement) and the measured ratios are more realistic. Therefore, the measurement results are used in our calculation. However, the spatiotemporal variation of NO_x/NO₂ ratios reported by the model can still be used as reference for our sensitivity analysis. The daily spatiotemporal variation (standard deviation) of NO_x/NO₂ ratios obtained from the model during the measurement campaign is treated as the uncertainty of the NO_x/NO₂ ratio. The variation of NO_x/NO₂ ratio is ranged from 0.10 to 0.36 with a mean value of 0.19. We took the 0.19 as the error of the NO_x/NO₂ ratio and propagate it in our emission calculation. The result shows the uncertainty of NO_x/NO₂ ratio would contribute to an error of 10.3%–16.3% (with an average value of 14.2%) in the NO_x emissions.

3.2.6. Total errors

We have discussed five major sources of error and their contributions to the NO_x emission calculation, the combined error can be calculated as follows:

$$\text{Error}_{\text{total}} = \sqrt{(\text{Error}_{VCD})^2 + (\text{Error}_{\text{gaps}})^2 + (\text{Error}_{\text{wind}})^2 + (\text{Error}_{\text{lifetime}})^2 + (\text{Error}_{\text{NO}_x/\text{NO}_2})^2} \quad (9)$$

Fig. 11 summarized the contribution of each source of error to the total NO_x emission for each of the measurement day. In general, the error caused by wind field and measurement gap dominated the total error. Other errors are comparably small. The total error of the NO_x emission ranges from 38.3% to 60.7%, with an average of 44.6%. Our result is comparable to previous studies which the error is ranging from 30% to 50% (Shaiganfar et al., 2011, 2017).

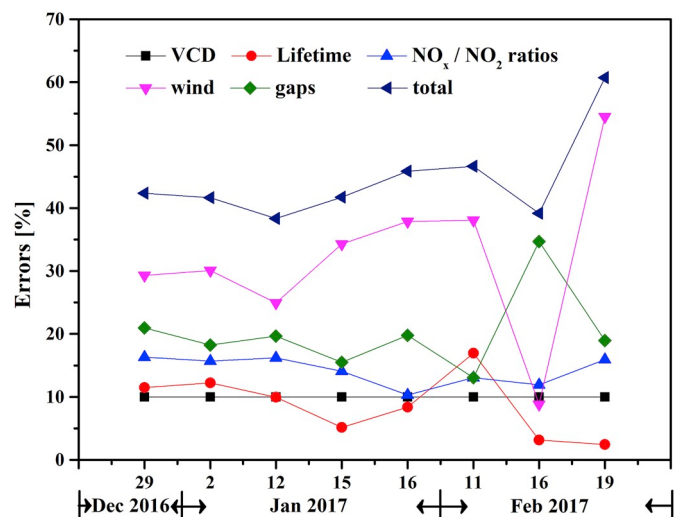


Fig. 11. The relative NO_x emissions errors contributed by NO₂ VCDs (black curve), measurement gaps (green curve), wind data (magenta curve), lifetime of NO_x (red curve), and NO_x/NO₂ ratios (blue curve). The total error is indicated by the navy curve. (For interpretation of the references to color in this figure legend, the reader is referred to the Web version of this article.)

3.3. Estimation of NO_x emission

In this study, 20 days of mobile MAX-DOAS measurements were performed. Some of the measurement days are not used for the flux estimation. It is mainly due to large measurement gaps and large variation of wind field. Details of the meteorological condition as well as the filter criteria for all measurements days are shown in Table 2 and Table 3. The inner route observation is close to the city center where the measurements were strongly influenced by various emission sources. The estimation of emissions is applied to the outer route where the influence from local emissions is less significant. In total, 8 days of outer route measurements are used for NO_x emissions calculation. The spatial distribution of NO₂ VCDs as well the wind information during these 8 days is shown in Fig. 12.

The NO_x emissions in Hefei were calculated following the procedure indicated in Section 2.6. Time series of the total NO_xemissions from areas within the outer route is shown in Fig. 13. The NO_xemission flux varies from $(10.25 \pm 4.70) \times 10^{24} \text{ molec s}^{-1}$ to $(40.28 \pm 17.06) \times 10^{24} \text{ molec s}^{-1}$ with a mean value of $(18.44 \pm 8.09) \times 10^{24} \text{ molec s}^{-1}$ (about 4.76 ton h^{-1}). The maximum NO_x emissions of $(40.28 \pm 17.06) \times 10^{24} \text{ molec s}^{-1}$ (~2.18 times of the average) was measured on 29 December 2016, the high NO_x emission can be explained by the enhanced emission in the city center. As shown in Fig. 3, high NO₂ VCDs were detected along the inner route. The increase of emission is likely related to the enhancement of traffic in the city before the long New Year holiday. The estimated NO_x emissions in mid-January of 2017 is rather stable at around $(11.51 \pm 1.12) \times 10^{24} \text{ molec s}^{-1}$. This is mainly due to the stable meteorological conditions and constant emissions during the time. An

Table 2
Measurement data filter criteria.

Problems	Criterion
VCD distribution	$\text{VCD}_{\text{up-wind}} > \text{VCD}_{\text{down-wind}}$
Gaps	Gaps $> 10 \text{ km};$
Wind	Low wind speed $< 2.0 \text{ ms}^{-1}$; Deviation of wind direction $> 30^\circ$
NO _x /NO ₂ ratios	NO _x /NO ₂ ratios > 2.0
Lifetime correction	Lifetime correction factor > 1.6

Table 3

Summary of the mobile MAX-DOAS measurements. Wind data is taken from WRF model simulation.

	Date (yyyy-mm-dd)	Wind Direction (°)	Wind Speed (ms ⁻¹)	Do Flux (yes/no)	Filtering principles
1	2016-12-19	73.09 ± 2.36	2.54 ± 0.44	No	Gaps
2	2016-12-29	33.02 ± 4.88	2.98 ± 0.14	Yes	
3	2016-12-30	195.41 ± 45.15	1.19 ± 0.68	No	VCD distribution, Wind, Lifetime correction
4	2016-12-31	154.88 ± 18.76	0.78 ± 0.41	No	Wind, Lifetime correction
5	2017-01-01	195.82 ± 3.61	2.61 ± 0.36	No	Gaps
6	2017-01-02	329.54 ± 5.79	2.99 ± 0.12	Yes	
7	2017-01-12	276.08 ± 4.61	3.71 ± 0.41	Yes	
8	2017-01-13	301.16 ± 2.46	5.65 ± 0.37	No	VCD distribution, NO _x /NO ₂ ratios
9	2017-01-14	67.25 ± 4.25	5.77 ± 54	No	VCD distribution
10	2017-01-15	89.82 ± 3.80	6.98 ± 0.81	Yes	
11	2017-01-16	105.70 ± 4.20	4.29 ± 0.26	Yes	
12	2017-02-10	320.64 ± 1.46	6.61 ± 0.46	No	Gaps
13	2017-02-11	231.92 ± 5.46	2.18 ± 0.26	Yes	
14	2017-02-12	183.49 ± 6.89	2.96 ± 0.21	No	Gaps,
15	2017-02-13	196.54 ± 8.68	1.50 ± 0.48	No	Wind, Lifetime correction
16	2017-02-14	113.30 ± 1.83	6.87 ± 0.44	No	Gaps,
17	2017-02-15	229.92 ± 5.34	2.92 ± 0.19	No	Gaps
18	2017-02-16	213.54 ± 2.07	11.04 ± 1.53	Yes	
19	2017-02-18	138.56 ± 5.86	1.95 ± 0.12	No	Wind, Lifetime correction
20	2017-02-19	217.58 ± 1.37	14.38 ± 1.75	Yes	

enhanced emission of NO_x was measured on 16 of February, the high value could be partly related to a rather large measurement gap on that measurement day. However, the error bar does not overlap with the measurement in mid January, indicating a significant enhancement of emission on this 16 of February. This is likely associated with the increase of workload factories in handling the backlog of work accumulated during the long Chinese New Year holiday. In addition, a significant "holiday effects" can also be observed from the NO_x emissions results. The emissions decreased from $(40.28 \pm 17.06) \times 10^{24}$ molec^s⁻¹ to $(22.13 \pm 9.21) \times 10^{24}$ molec^s⁻¹ for measurements performed on 29 December 2016 and 2 January 2017 (New Year holiday). In addition, the NO_x emission dropped from $(23.18 \pm 9.08) \times 10^{24}$ molec^s⁻¹ to $(15.55 \pm 9.45) \times 10^{24}$ molec^s⁻¹ for measurements taken on 16 and 19 February 2017 (Sunday). During this campaign, the averaged NO_x emission measured during weekdays is $21.40 \pm 13.84) \times 10^{24}$ molec^s⁻¹ and reduced by 28% to $(15.49 \pm 4.71) \times 10^{24}$ molec^s⁻¹ during weekend and holidays.

Assuming the average of NO_x emission measured during the campaign is representative for Hefei for the entire year, the annual NO_x emission would be 41.73×10^3 ton year⁻¹. As the measurements were taken in winter which the emission is expected to be higher due to the increase in domestic heating emissions. Our estimation might overestimate the annual average NO_x emission. However, our result is still ~43% lower than the estimation from the Multiresolution Emission Inventory for China (MEIC) model v1.2 ($0.25^\circ \times 0.25^\circ$, monthly mean; available at <http://www.meicmodel.org>) emission inventory which the NO_x emission of outer measurement route encircled areas was estimated to be 73.16×10^3 ton year⁻¹ in 2012. Reduction of NO_x emission is mainly due to the government strengthened the emission control

measures in recent years. In addition, with the development and expansion of the city, some heavy polluting factories or even the power plant were moved out from the city, i.e., the power plant located outside the outer route (point F in Fig. 2). The reducing trend of NO_x emissions matches with previous study in China (Liu et al., 2017). Comparing our estimation to previous studies in other cities around the world, the magnitude of total NO_x emission in Hefei is slightly lower than the NO_x emission of 51.42×10^3 ton year⁻¹ in Guangzhou, China (Wu et al., 2013) and much lower than that of St. Petersburg (NO_x emissions of $\sim 60 \times 10^3$ ton year⁻¹) (Ionov and Poberovskii, 2018), Beijing (NO₂ emissions of 62.76×10^3 ton year⁻¹) (Li et al., 2015) and Paris (NO_x emissions of $88.25\text{--}152.24 \times 10^3$ ton year⁻¹) (Shaiganfar et al., 2017).

Apart from emission estimation, the mobile measurement data can also be used to investigate the transportation of pollutants and their impacts on local air quality. We can estimate the contribution of transported pollutants by taking the ratio of the influx (pollutants transport into the city) and outflux (pollutants going out from the city). During the measurement campaign, the influx varies from $(19.57 \pm 9.13) \times 10^{24}$ molec^s⁻¹ to $(114.34 \pm 69.45) \times 10^{24}$ molec^s⁻¹ with an average value of $(57.26 \pm 26.80) \times 10^{24}$ molec^s⁻¹ while the out flux varies from $(31.44 \pm 14.66) \times 10^{24}$ molec^s⁻¹ to $(129.89 \pm 78.89) \times 10^{24}$ molec^s⁻¹, with the mean value of $(75.70 \pm 34.90) \times 10^{24}$ molec^s⁻¹. It is important to notice the large contribution of incoming NO_x pollution. The incoming NO_x is about 3.10 times larger than the local emissions of the city. As the measurement campaign was took place during winter, a high season of energy consumption in the northern China due to domestic heating. On the other hand, domestic heating emissions in Hefei are expected to be much lower than that in the northern China. In addition, the prevailing

Table 4

NO_x emissions from the Ring Expressway encircled area, influx, outflux and the ratios of emissions to outflux are also present.

Date (yyyy-mm-dd)	Time, LT (hh:mm-hh:mm)	C _{life}	C _L	Influx (10^{24} molec ^s ⁻¹)	Outflux (10^{24} molec ^s ⁻¹)	Emissions (10^{24} molec ^s ⁻¹)	Influx/Outflux (%)
2016-12-29	11:51–14:35	1.34	1.19	46.53	86.80	40.28	53.60
2017-01-02	12:15–14:57	1.37	1.25	40.68	62.80	22.13	64.77
2017-01-12	10:28–13:15	1.29	1.21	32.37	44.25	11.88	73.16
2017-01-15	08:49–11:44	1.14	1.39	50.91	63.32	12.41	80.40
2017-01-16	08:50–11:33	1.24	1.89	80.34	90.59	10.25	88.68
2017-02-11	12:27–15:11	1.53	1.09	19.57	31.44	11.87	62.25
2017-02-16	10:22–13:06	1.09	1.06	73.32	96.50	23.18	75.98
2017-02-19	10:00–12:41	1.07	1.18	114.34	129.89	15.55	88.03

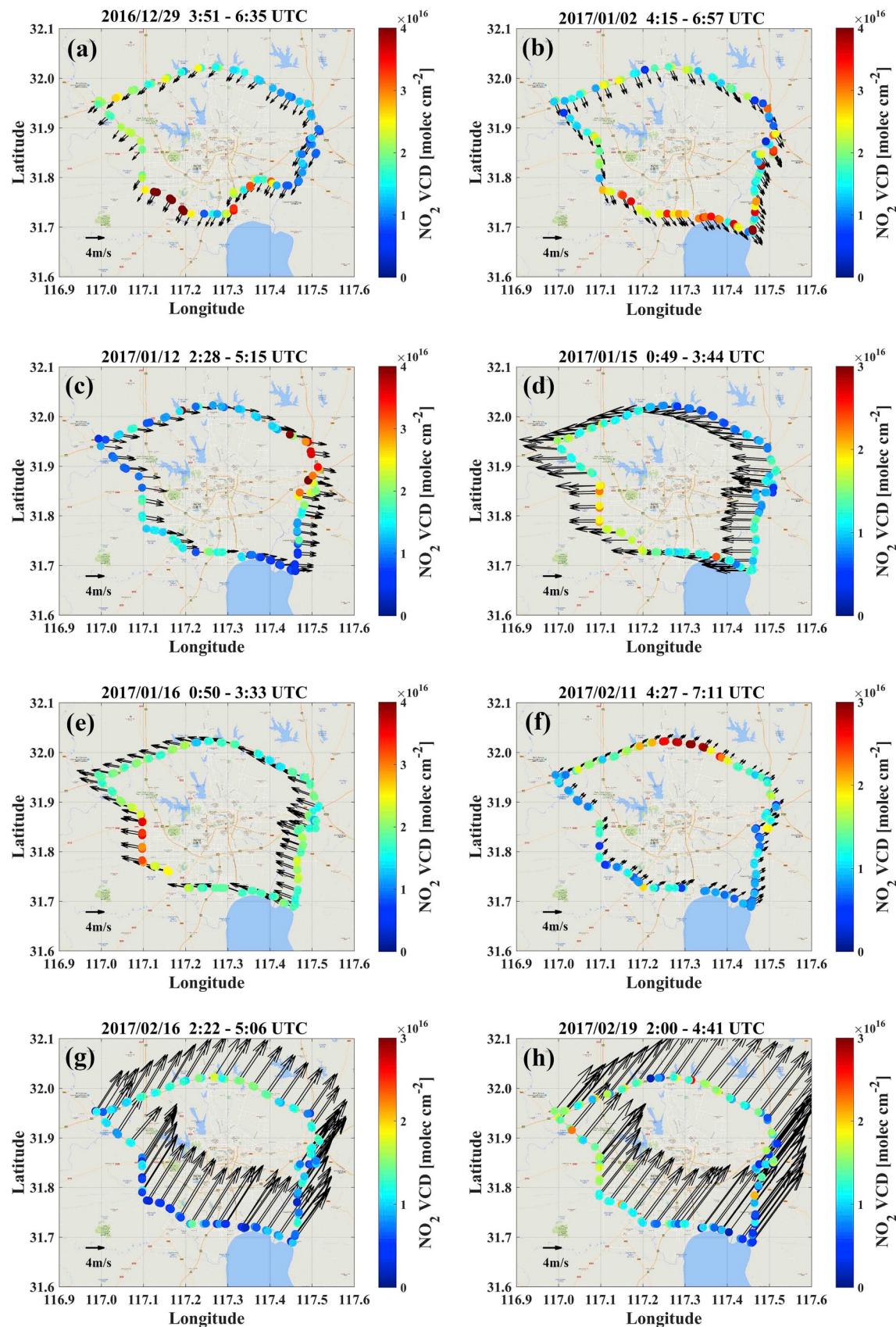


Fig. 12. Spatial distribution of NO_2 VCDs and the wind information of the 8 measurement days.

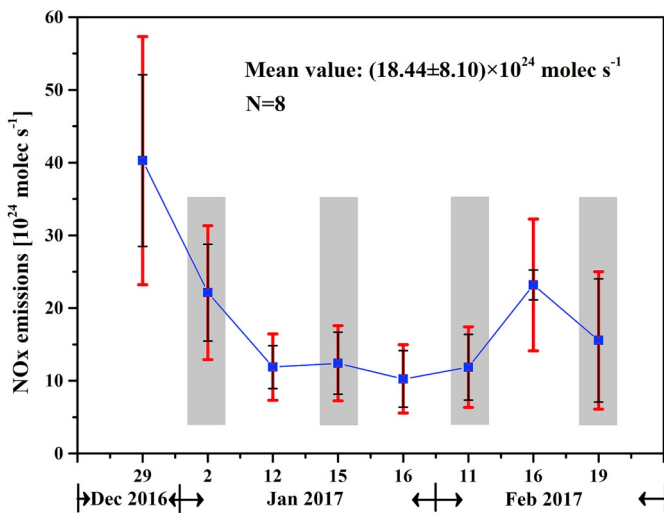


Fig. 13. Time series of the total NO_x emission in Hefei retrieved from the mobile MAX-DOAS measurements. The averaged total NO_x emissions is $(18.44 \pm 8.10) \times 10^{24}$ molec s^{-1} . The red error bars indicate the total uncertainties while the black error bars represent the uncertainty caused by wind field. In addition, the measurements performed on weekend and holiday periods are marked with grey shades. (For interpretation of the references to color in this figure legend, the reader is referred to the Web version of this article.)

wind direction of Hefei during wintertime is northeasterly. Therefore, it is expected to have stronger influence from pollutants coming from the north. Besides, air quality of Hefei is also significant influenced by regional transport of pollutants from Yangtze River Delta, a highly industrialized and heavily polluted area (see Fig. 1). The impact on the air quality is also notable during easterly wind conditions in winter. Details of the in and out flux of NO_x of each measurement day are shown in Table 4. As the outflux includes the transportation (influx) and the city emission, we calculated the ratio of influx to outflux to analysis the contribution of transportation to the total outflux. The averaged value of the ratios of influx to outflux is 73.4% during this campaign. The result implies 73.4% of NO_x is coming from area outside the outer route. Note that this number is based on measurements during winter time and the annual average value is expected to be smaller. The result indicates that pollutants originated from long range transport from upwind areas show a significant impact on the air quality of Hefei. Our analysis provided a quantitative estimation of the influence of regional air mass transport on the local air quality in Hefei during winter time.

4. Summary and conclusions

In this paper, we present a quantitative determination of the NO_x emission in Hefei using mobile MAX-DOAS measurements. The measurements were carried out during winter time from December 2016 to February 2017. Mobile MAX-DOAS measurements were taken along the Second Ring Road (inner route) and the Ring Expressway (outer route) of the city. The mobile measurements of NO₂ show a clear spatial dependency with higher NO₂ VCDs along the inner route and lower values over the outer route, indicating the majority of NO_x emission sources are located at the city center. A significant “holiday effect” was found by comparing measurements taken during weekdays and weekend. The NO₂ VCDs observed during weekend are in general reduced by 28% along the outer, while a less significant reduction of 13% was measured in the city center.

The mobile MAX-DOAS measurements of NO₂ were also compared to the stationary MAX-DOAS located at the city center. NO₂ VCDs reported from these two instruments show a good agreement with a Pearson correlation coefficient R of 0.77 for mobile measurement along the inner route. The correlation reduced to 0.62 for measurement along

the outer route, indicating the strong spatial gradient of NO₂ over the city. The mobile measurements are also compared to OMI satellite observations. In general, a good agreement was found between mobile MAX-DOAS and OMI observations with correlation coefficient R of 0.89. However, OMI is underestimating the tropospheric NO₂ VCD by 19%. The discrepancy is mainly due to the differences in spatial and temporal coverage between 2 measurements.

The loop-integral method was applied to the mobile MAX-DOAS NO_x measurements to calculate the total NO_x emission of Hefei. This method relies on the input of meteorological data, vertical distribution of NO₂, assumption of NO_x atmospheric lifetime as well as the NO_x/NO₂ ratios. All these inputs are associated with errors, and could result in large uncertainty in the emission estimation. Therefore, we performed a detailed sensitivity analysis to determine the major sources of error and their impacts on the emission result. The result shows the total error of NO_x emission ranges from 38 to 61% with an average value of 45%, and the error is dominated by the variation of wind field and measurement gap.

Our result shows the NO_x emission in Hefei during winter time varies in a wide range from 10×10^{24} to 40×10^{24} molec s^{-1} with an average of 18.44×10^{24} molec s^{-1} . Assuming our measurement is representative for the entire year, we can simply convert to an annual emission of 41.73×10^{3} ton year $^{-1}$. Our estimation is about 43% lower than the number reported in the previous emission inventory in 2012. The reduction of NO_x emission is mainly due to the strengthened emission control measures in recent years. In addition, some heavy polluted industries and power plants were moved away from the city to the suburban areas. Our measurement data can also be used to estimate the influence of transported pollutants on the local air quality. About 73% of the NO_x measured in the city were transported from areas outside the outer route. The impacts of transported NO_x are especially large when the air masses originated from the polluted North China Plain and Yangtze River Delta. Our result provided a quantitative estimation of local emission of NO_x as well as the influences of regional air mass transport on local air quality in Hefei during winter time. This information is useful for urban development and planning as well as the design of air pollution control policies in the future.

Declarations of interest

None.

Acknowledgements

This work is jointly supported by grants from National Key Research and Development Program of China (2018YFC0213104, 2018YFC0213100, 2016YFC0203302), National Natural Science Foundation of China (41722501, 91544212, 51778596, 41575021) and the National High-Resolution Earth Observation Project of China under Grant 05-Y20A16-9001-15/17-2. We thank the National Oceanic and Atmospheric Administration (NOAA) Air Resources Laboratory (ARL) for the provision of the HYSPLIT transport and dispersion model used in this publication.

References

- Ångström, A., 1929. On the atmospheric transmission of sun radiation and on dust in the air. *Geogr. Ann.* 11, 156–166.
- Beirle, S., Boersma, K.F., Platt, U., Lawrence, M.G., Wagner, T., 2011. Megacity emissions and lifetimes of nitrogen oxides probed from space. *Science* 333, 1737–1739.
- Beirle, S., Platt, U., Wenig, M., Wagner, T., 2003. Weekly cycle of NO₂ by GOME measurements: a signature of anthropogenic sources. *Atmos. Chem. Phys.* 3, 2225–2232.
- Bucsela, E.J., Krotkov, N.A., Celarier, E.A., Lamsal, L.N., 2013. A new stratospheric and tropospheric NO₂ retrieval algorithm for nadir-viewing satellite instruments: applications to OMI. *Atmos. Meas. Tech.* 6, 2607–2626.
- Chan, K.L., Hartl, A., Lam, Y.F., Xie, P.H., Liu, W.Q., Cheung, H.M., Lampel, J., Pöhler, D., Li, A., Xu, J., Zhou, H.J., Ning, Z., Wenig, M.O., 2015. Observations of tropospheric NO₂ using ground based MAX-DOAS and OMI measurements during the Shanghai

- World Expo 2010. *Atmos. Environ.* 119, 45–58.
- Chan, K.L., Wiegner, M., Wenig, M., Pöhler, D., 2017. Observations of tropospheric aerosols and NO₂ in Hong Kong over 5 years using ground based MAX-DOAS. *Sci. Total Environ.* 619–620, 1545–1556.
- Chance, K., Kurucz, R.L., 2010. An improved high-resolution solar reference spectrum for earth's atmosphere measurements in the ultraviolet, visible, and near infrared. *J. Quant. Spectrosc. Radiat. Transfer* 111, 1289–1295.
- Chance, K.V., Spurr, R.J., 1997. Ring effect studies: Rayleigh scattering, including molecular parameters for rotational Raman scattering, and the Fraunhofer spectrum. *Appl. Opt.* 36, 5224–5230.
- Clémér, K., Van Roozendael, M., Fayt, C., Hendrick, F., Hermans, C., Pinardi, G., Spurr, R., Wang, P., De Mazière, M., 2010. Multiple wavelength retrieval of tropospheric aerosol optical properties from MAXDOAS measurements in Beijing. *Atmos. Meas. Tech.* 3, 863–878.
- Foy, B.D., Molina, L.T., Molina, M.J., 2006. Satellite-derived land surface parameters for mesoscale modelling of the Mexico City basin. *Atmos. Chem. Phys.* 6, 1315–1330.
- Frieß, U., Klein Baltink, H., Beirle, S., Clémér, K., Hendrick, F., Henzing, B., Irie, H., de Leeuw, G., Li, A., Moerman, M.M., van Roozendael, M., Shaiganfar, R., Wagner, T., Wang, Y., Xie, P., Yilmaz, S., Zieger, P., 2016. Intercomparison of aerosol extinction profiles retrieved from MAX-DOAS measurements. *Atmos. Meas. Tech.* 9, 3205–3222.
- Frieß, U., Monks, P., Remedios, J., Rozanov, A., Sinreich, R., Wagner, T., Platt, U., 2006. MAX-DOAS O4 measurements: a new technique to derive information on atmospheric aerosols: 2. Modeling studies. *J. Geophys. Res.: Atmosphere* 111.
- Frieß, U., Sihler, H., Sander, R., Pöhler, D., Yilmaz, S., Platt, U., 2011. The vertical distribution of BrO and aerosols in the Arctic: measurements by active and passive differential optical absorption spectroscopy. *J. Geophys. Res.: Atmosphere* 116.
- Hendrick, F., Müller, J.F., Clémér, K., Wang, P., De Mazière, M., Fayt, C., Gielen, C., Hermans, C., Ma, J.Z., Pinardi, G., Stavrakou, T., Vlemmix, T., Van Roozendael, M., 2014. Four years of ground-based MAX-DOAS observations of HONO and NO₂ in the Beijing area. *Atmos. Chem. Phys.* 14, 765–781.
- Hong, Q., Liu, C., Chan, K.L., Hu, Q., Xie, Z., Liu, H., Si, F., Liu, J., 2018. Ship-based MAX-DOAS measurements of tropospheric NO₂, SO₂, and HCHO distribution along the Yangtze River. *Atmos. Chem. Phys.* 18, 5931–5951.
- Ibrahim, O., Shaiganfar, R., Sinreich, R., Stein, T., Platt, U., Wagner, T., 2010. Car MAX-DOAS measurements around entire cities: quantification of NO_x emissions from the cities of Mannheim and Ludwigshafen (Germany). *Atmos. Meas. Tech.* 3, 709–721.
- Ionov, D., Poberovskii, A., 2018. Observations of urban NO_x plume dispersion using mobile and satellite DOAS measurements around the megacity of St.Petersburg (Russia). *Int. J. Rem. Sens.* 3–15.
- Jang, M., Kamens, R.M., 2001. Characterization of secondary aerosol from the photo-oxidation of toluene in the presence of NO_x and 1-propene. *Environ. Sci. Technol.* 35, 3626–3639.
- Johansson, M., Galle, B., Yu, T., Tang, L., Chen, D., Li, H., Li, J.X., Zhang, Y., 2008. Quantification of total emission of air pollutants from Beijing using mobile mini-DOAS. *Atmos. Environ.* 42, 6926–6933.
- Krotkov, N.A., Lamsal, L.N., Celerier, E.A., Swartz, W.H., Marchenko, S.V., Bucsela, E.J., Chan, K.L., Wenig, M., Zara, M., 2017. The version 3 OMI NO₂ standard product. *Atmos. Meas. Tech.* 10, 3133–3149.
- Kuhlmann, G., Hartl, A., Cheung, H.M., Lam, Y.F., Wenig, M.O., 2014. A novel gridding algorithm to create regional trace gas maps from satellite observations. *Atmos. Meas. Tech.* 7, 451–467.
- Levert, P.F., Oord, G.H.J.V.D., Dobber, M.R., Malkki, A., Visser, H., Vries, J.D., Stammes, P., Lundell, J.O.V., Saari, H., 2006. The ozone monitoring instrument. *IEEE Trans. Geosci. Rem. Sens.* 44, 1093–1101.
- Li, A., Zhang, J., Xie, P., Hu, Z., Xu, J., Mou, F., Wu, F., Liu, J., Liu, W., 2015. Variation of temporal and spatial patterns of NO₂ in Beijing using OMI and mobile DOAS. *Sci. China Chem.* 58, 1367–1376.
- Lin, J.-T., 2012. Satellite constraint for emissions of nitrogen oxides from anthropogenic, lightning and soil sources over East China on a high-resolution grid. *Atmos. Chem. Phys.* 12, 2881–2898.
- Lin, J.-T., McElroy, M.B., 2011. Detection from space of a reduction in anthropogenic emissions of nitrogen oxides during the Chinese economic downturn. *Atmos. Chem. Phys.* 11, 8171–8188.
- Lin, J.T., McElroy, M.B., Boersma, K.F., 2010. Constraint of anthropogenic NO_x emissions in China from different sectors: a new methodology using multiple satellite retrievals. *Atmos. Chem. Phys.* 9, 63–78.
- Liu, F., Beirle, S., Zhang, Q., Dörner, S., He, K., Wagner, T., 2016a. NO_x lifetimes and emissions of cities and power plants in polluted background estimated by satellite observations. *Atmos. Chem. Phys.* 16, 5283–5298.
- Liu, F., Beirle, S., Zhang, Q., van der, A.R., Zheng, B., Tong, D., He, K., 2017. NO_x emission trends over Chinese cities estimated from OMI observations during 2005 to 2015. *Atmos. Chem. Phys.* 17, 9261–9275.
- Liu, H., Cheng, L., Xie, Z., Ying, L., Xin, H., Wang, S., Jin, X., Xie, P., 2016b. A paradox for air pollution controlling in China revealed by “APEC Blue” and “Parade Blue”. *Sci. Rep.* 6, 34408.
- Platt, U., Stutz, J., 2008. Differential Optical Absorption Spectroscopy. Springer Berlin Heidelberg.
- Rodgers, C.D., 2000. Inverse Methods for Atmospheric Sounding: Theory and Practice. World scientific.
- Rothman, L.S., Rinsland, C.P., Goldman, A., Massie, S.T., Edwards, D.P., Flaud, J.M., Perrin, A., Camy-Peyret, C., Dana, V., Mandin, J.Y., 2010. The hitran molecular spectroscopic database and hawks (hitran atmospheric workstation): 1996 edition (reprint from J quant spectrosc radiat transfer, vol 60, pg 665-710, 1998). *J. Quant. Spectrosc. Radiat. Transfer* 111, 1568–1613.
- Rozanov, A., Rozanov, V., Buchwitz, M., Kokhanovsky, A., Burrows, J.P., 2005. SCITRAN 2.0 – a new radiative transfer model for geophysical applications in the 175–2400 nm spectral region. *Adv. Space Res.* 36, 1015–1019.
- Seinfeld, J.H., Pandis, S.N., 2006. From air pollution to climate change. *Atmos. Chem. Phys.* 429–443.
- Seinfeld, J.H., Pandis, S.N., 2012. Atmospheric Chemistry and Physics: from Air Pollution to Climate Change, second ed. .
- Serdyuchenko, A., Gorshelev, V., Weber, M., Chehade, W., Burrows, J.P., 2014. High spectral resolution ozone absorption cross-sections - Part 2: temperature dependence. *Atmos. Meas. Tech.* 7, 625–636.
- Shaiganfar, R., Beirle, S., Denier van der Gon, H., Jonkers, S., Kuennen, J., Petetin, H., Zhang, Q., Beekmann, M., Wagner, T., 2017. Estimation of the Paris NO_x emissions from mobile MAX-DOAS observations and CHIMERE model simulations during the MEGAPOLI campaign using the closed integral method. *Atmos. Chem. Phys.* 17, 7853–7890.
- Shaiganfar, R., Beirle, S., Sharma, M., Chauhan, A., Singh, R.P., Wagner, T., 2011. Estimation of NO_x emissions from Delhi using Car MAX-DOAS observations and comparison with OMI satellite data. *Atmos. Chem. Phys.* 11, 10871–10887.
- Solomon, S., Portmann, R.W., Sanders, R.W., Daniel, J.S., Madsen, W., Bartram, B., Dutton, E.G., 1999. On the role of nitrogen dioxide in the absorption of solar radiation. *J. Geophys. Res. Atmos.* 104, 12047–12058.
- Stein, A.F., Draxler, R.R., Rolph, G.D., Stunder, B.J.B., Cohen, M.D., Ngan, F., 2016. NOAA's HYSPLIT atmospheric transport and dispersion modeling system. *Bull. Am. Meteorol. Soc.* 96, 150504130527006.
- Su, W., Liu, C., Hu, Q., Fan, G., Xie, Z., Huang, X., Zhang, T., Chen, Z., Dong, Y., Ji, X., Liu, H., Wang, Z., Liu, J., 2017. Characterization of ozone in the lower troposphere during the 2016 G20 conference in Hangzhou. *Sci. Rep.* 7, 17368.
- Tan, W., Liu, C., Wang, S., Xing, C., Su, W., Zhang, C., Xia, C., Liu, H., Cai, Z., Liu, J., 2018. Tropospheric NO₂, SO₂, and HCHO over the East China Sea, using ship-based MAX-DOAS observations and comparison with OMI and OMPS satellites data. *Atmos. Chem. Phys.* 18, 15387–15402.
- Thalman, R., Volkamer, R., 2013. Temperature dependent absorption cross-sections of O₂-O₂ collision pairs between 340 and 630 nm and at atmospherically relevant pressure. *Phys. Chem. Chem. Phys. Cpcp* 15, 15371–15381.
- Tzanis, C., Varotsos, C., Ferm, M., Christodoulakis, J., 2009. Nitric acid and particulate matter measurements at Athens, Greece, in connection with corrosion studies. *Atmos. Chem. Phys.* 9, 8309–8316.
- Vandaele, A.C., Hermans, C., Simon, P.C., Carleer, M., Colin, R., Fally, S., Mérianne, M.F., Jenouvrier, A., Coquart, B., 1998. Measurements of the NO₂ absorption cross-section from 42000 cm⁻¹ to 10000 cm⁻¹ (238–1000 nm) at 220 K and 294 K. *J. Quant. Spectrosc. Radiat. Transfer* 59, 171–184.
- Vlemmix, T., Hendrick, F., Pinardi, G., De Smedt, I., Fayt, C., Hermans, C., Piters, A., Wang, P., Levelt, P., Van Roozendael, M., 2015. MAX-DOAS observations of aerosols, formaldehyde and nitrogen dioxide in the Beijing area: comparison of two profile retrieval approaches. *Atmos. Meas. Tech.* 8, 941–963.
- Wang, S., Zhou, B., Wang, Z., Yang, S., Hao, N., Valks, P., Trautmann, T., Chen, L., 2012. Remote sensing of NO₂ emission from the central urban area of Shanghai (China) using the mobile DOAS technique. *J. Geophys. Res.: Atmosphere* 117, D13305.
- Wu, F.C., Xie, P.H., Li, A., Chan, K.L., Hartl, A., Wang, Y., Si, F.Q., Zeng, Y., Qin, M., Xu, J., Liu, J.G., Liu, W.Q., Wenig, M., 2013. Observations of SO₂ and NO₂ by mobile DOAS in the Guangzhou eastern area during the asian games 2010. *Atmos. Meas. Tech.* 6, 2277–2292.
- Xing, C., Liu, C., Wang, S., Chan, K.L., Gao, Y., Huang, X., Su, W., Zhang, C., Dong, Y., Fan, G., Zhang, T., Chen, Z., Hu, Q., Su, H., Xie, Z., Liu, J., 2017. Observations of the vertical distributions of summertime atmospheric pollutants and the corresponding ozone production in Shanghai, China. *Atmos. Chem. Phys.* 17, 14275–14289.